TOWARDS IMAGING SKIN CANCER BY APERTURELESS SCANNING NEAR-FIELD OPTICAL MICROSCOPY

Stefan G. STANCIU[1*], Mariana COSTACHE[2], Denis E. TRANCA[1], Radu HRISTU[1], Marius POPESCU[1,3], Valentin ENACHE[3] and George A. STANCIU[1]

Laser Scanning Microscopy Techniques such as Confocal Microscopy, Two Photon Excitation Microscopy, Second Harmonic Generation Microscopy or Fluorescence Lifetime Imaging have been successfully employed to date for imaging skin cancer. However, the resolution that such techniques can provide is limited by diffraction, which prevents accurately imaging (and differentiating) optical details sized below ~200nm, which could potentially advance our current understanding of skin cancer progression or causes. In this paper we present the results of our first efforts on imaging tissue samples relevant for skin cancer research at optical resolutions beyond the diffraction limit by using Apertureless Scanning Near-Field Optical Microscopy.

Keywords: ASNOM, CLSM, skin cancer, squamous cell carcinoma, microscopy, nanoscopy.

1. Introduction

Laser Scanning Microscopy (LSM) techniques play a key role in understanding the cellular structures specific to cancer tumors, including those specific to skin cancer, the most common form of human cancer. For example, Confocal Laser Scanning Microscopy (CLSM) was demonstrated to be a useful adjunct to clinical histopathology, allowing for identification of malignant cells and small tumor nests in vivo based on the reflective properties of human tissue [1]. Two-Photon Excitation Fluorescence Microscopy (TPEF) or Second Harmonic Generation Microscopy (SHG) have been found as well to be highly suitable for investigating skin tissue in the absence of artificial markers [2; 3], as multiple endogenous fluorophores present in the human skin tissue, such as keratin, nicotinamide adenine dinucleotide, collagen, melanin, or tryptophan, can be excited by TPEF and collagen interfaces exhibit strong SHG signal. The possibilities that Fluorescence Lifetime Imaging (FLIM) provides for profiling

[1] Center for Microscopy-Microanalysis and Information Processing, University Politehnica of Bucharest, Splaiul Independentei 313, Bucharest, Romania
[2] "Carol Davila' University of Medicine and Pharmacy, Eroii Sanitari 8, Bucharest, Romania
[3] Clinical Emergency Hospital Bucharest, Calea Floreasca 8, Bucharest, Romania
Corresponding author's e-mail: stefan.stanciu@cmmip-upb.org

different tissue architectures based on the emission lifetime of endogenous fluorophores has been as well successfully exploited to date in the purpose of skin cancer diagnostic [4].

Although the above mentioned LSM techniques represent very powerful tools for understanding and diagnosing skin cancer, their resolution is however limited by diffraction, which prevents accurately imaging (or differentiating) sub-cellular details sized below 200nm. Resolving such nanoscaled features could potentially advance our current understanding of skin cancer progression and causes. Non-optical imaging techniques such as Scanning Electron Microscopy or Atomic Force Microscopy provide nanoscale resolutions suitable for studying morpho-structural characteristics of skin tissue samples that are sized below 200nm, but their contrast mechanisms make these techniques unable to provide any optical information, which is typically required by pathologists for establishing a diagnostic. A series of super-resolution laser scanning techniques have emerged in the last two decades, such as Stimulated Emission Depletion Microscopy (STED), Fluorescence Photo Activation Localization Microscopy (f-PALM) or Stochastic Optical Reconstruction Microscopy (STORM), succeeding in overcoming the resolution limits imposed by diffraction, offering routine resolutions of ~50nm, and up to 10nm in special configurations, but these techniques are fluorescence based and thus cannot be used for imaging samples that are not labeled with specially designed contrast agents. Optical resolutions in the same range have become available as well by a hybrid family of scanning probe techniques, Apertureless Scanning Near-Field Optical Microscopy (ASNOM). ASNOM techniques offer optical information from the near-field of the sample at sub-wavelength resolutions theoretically limited only by the dimension of a metallic tip that needs to be scanned across the sample surface while being illuminated by a laser beam. In this study we introduce the concept of imaging skin tissue at optical resolutions below the diffraction limit using ASNOM, we present an imaging protocol based on far-field techniques and ASNOM with potential for facilitating the correlation of micro- and nano-scale data and present a set of initial results on this subject, discussing as well limitations of this approach and future directions.

The outline of the paper is as follows. The working principle of ASNOM imaging is presented in Section 2. In section 3 we present the ASNOM system that we used for image acquisition, while the experimental results are presented in Section 4. Finally, the conclusions are drawn in Section 5.

2. Working Principles of Apertureless Scanning Near-Field Optical Microscopy

ASNOM represents a family of techniques based on scanning a sharp nanoscale probe (e.g. cantilever tip) across a sample while illuminating the probe, or the sample region underneath, using a laser beam. Different ASNOM techniques rely on different contrast mechanisms and provide complementary optical information. The most popular ASNOM variant is scattering-type Scanning Near-Field Optical Microscopy (s-SNOM), which exploits the field enhancing nano-antenna properties of sharp metallic tips [5]. More precisely, it exploits the fact that scatterers at the apex of a metallic nano tip induce near-field electromagnetic interaction with the surface of the investigated sample, and this interaction influences the radiation that is elastically scattered into the far-field from the tip-apex. The resolution achievable by s-SNOM is directly linked to the radius of the metallic tip that is scanned across the sample surface, and can reach values even lower than 10 nm. A Fluorescence Apertureless Scanning Near-Field Optical Microscope (FASNOM) can be built on a similar architecture to the s-SNOM and can achieve a similar resolution (<10nm) for fluorescent samples. FASNOM exploits the fact that metallic structures have complex effects on fluorescence. More precisely, it relies on the fact that placing a metallic structure in the vicinity of a fluorophore leads to fluorescence quenching or enhancement and also to a modification of both the radiative and the non-radiative rates of the probe, inducing changes in both the fluorescence lifetime and the emission intensity [6]. Nonlinear approaches to ASNOM imaging have been as well reported in the literature. In the second-harmonic generation ASNOM (SHG-ASNOM) approach only the tip, or only the sample, needs to be SHG active to enable SHG-ASNOM imaging [7]. In different experimental SHG-ASNOM implementations, imaging is performed by measuring the local second harmonic field generated at a sample surface when the nonlinear susceptibility of a sample is higher than that of a probe tip.

3. Image Acquisition

The conducted investigations were performed by using a home-made system that combines a commercial Atomic Force Microscope (AFM), Quesant Q-Scope 350, and an ASNOM module built in-house, Fig. 1. In this configuration the excitation laser beam is focused through a long working distance objective (50x, 0.42 N.A.). For excitation we have used a semiconductor laser tuned at 638 nm with 0.5 mW power. The focal spot is aligned with the AFM probe, and the lateral position of the probe is controlled by closed-loop feedback. The objective collects optical near-field optical signals which are then directed onto a

photodiode. The system allows for simultaneous acquisition of AFM/ASNOM data, for AFM imaging the system performing in intermittent (tapping) mode.

The probe that we used in the case of the current experiment had an apex radius of curvature of ~30 nm and was made from silicon covered with two metallic layers, the first layer being Ti (15 nm) and the second one Pt (10 nm). The typical force constant of this cantilever is 0.15 Nm^{-1} and the typical resonant frequency is 55.5 kHz.

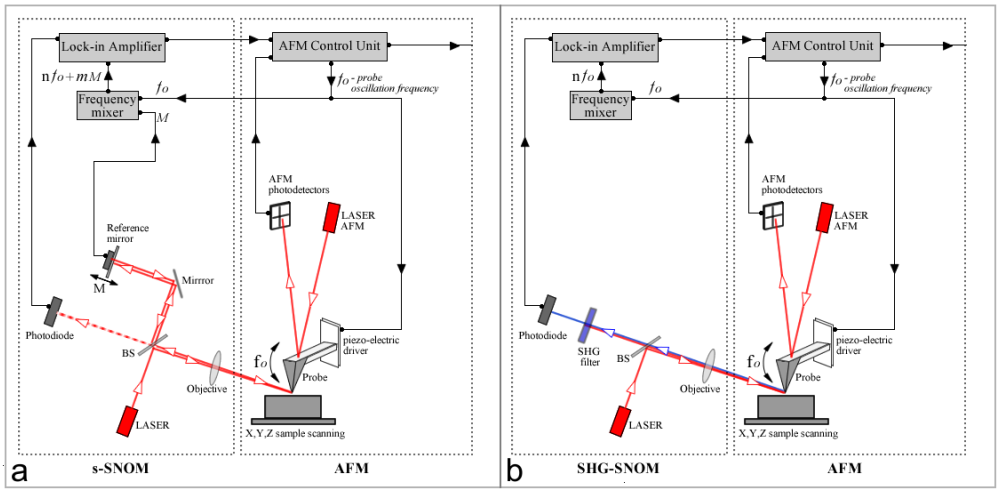

Fig. 1. ASNOM experimental setup. (a) The s-SNOM setup is based on a pseudo-heterodyne detection configuration [8], which consists in a Michelson interferometer with one interferometer arm focused onto the tip and the other one reflected off a harmonic oscillating reference mirror. The reference beam interferes with the scattered light originated from the near-field of the sample and the interference signal contains the near-field information at frequencies $n \cdot fo \pm m \cdot M$, where f_o is the probe oscillation frequency, M is the mirror oscillation frequency and n, m are integers. The s-SNOM signal is collected using a lock-in amplifier locked at the $n \cdot fo \pm m \cdot M$ spectral harmonics. (b) The SHG-SNOM setup shares common elements to the s-SNOM one but its configuration is simpler, as no interference between the probe beam and a reference beam is needed. A band pass filter centered at $\lambda/2$, where λ represents the wavelength used for excitation, is placed in this configuration before the detector in order to separate SHG signals from background.

A similar ASNOM imaging setup was also used for previous reported experiments such as ones focused on imaging fluorophore doped silica nanoparticles [9], or for determining the dielectric function of materials with nanoscale resolution [10]. For CLSM/TPEF experiments we used a Leica TCS SP system equipped with a Ti:Sapphire Laser (Tsunami, Spectraphysics).

4. Experimental Approach and Results

Squamous-cell carcinoma (SCC) represents one of the most common cutaneous neoplasms, these malignant tumors representing the second most frequent form of skin cancer. In the presented experiment we have employed a combined imaging approach for investigating paired skin tissue fragments, consecutively sliced from a formaldehyde-fixed and paraffin-embedded histological SCC skin tissue block. The histological tissue blocks used in the frame of our experiment had been previously collected from patients for routine histopathological examinations, and have been de-identified prior to the access by the authors. In the employed imaging strategy far-field information was collected using CLSM on tissue fragments stained with Hematoxylin-Eosin (HE) and also on their unstained pairs, which were also imaged with TPEF. Near-field information was collected only on the unstained instances using two ASNOM variants, s-SNOM and SHG-SNOM. The purpose of using four microscopy techniques was to identify corresponding regions of the HE-stained sample and its pair, and also to establish correspondences with histopathological relevance between the microscaled (CLSM, TPEF) and nanoscaled (s-SNOM, SHG-SNOM) image sets. Such correlative approaches hold potential for resolving the interpretation of nanoscaled data, as data collected using mature LSM techniques is more accessible in terms of interpretation by trained pathologists, while potentially sharing common elements with data collected using optical nanoscopy techniques (depending on the associated contrast mechanisms). In the case of the our experiment, CLSM was used to support ASNOM investigations because under adequate illumination settings micrographs collected by fluorescence CLSM on HE stained samples correlate well to micrographs collected using conventional optical microscopes (e.g. [11]), which are traditionally used in histopathology assays. The presence of fluorescent signals corresponding to HE staining in the CLSM images leads to their straightforward interpretation by using standard histopathology cues.

In Fig. 2.a) we present a 1 mm x 1 mm CLSM image collected using a 10X objective on a HE stained tissue fragment affected by SCC. The fluorescence signals recorded under the 488nm illumination setting that we have used correspond to Eosin, but also to the endogenous tissue chromophores with absorption spectra matching the above mentioned wavelength, flavins, carotenoids and bilirubin. For the considered region we aimed to find its correspondent on the unstained slide. In this purpose, CLSM under the same illumination setting was conducted on the unstained samples to collect fluorescence information that could be exploited for registering the imaged regions. In Fig. 2.b) we present a CLSM micrograph collected on the corresponding field of view, under the same acquisition conditions, on the unstained instance in the pair. The signals recorded

in this image correspond solely to the previously mentioned endogenous chromophores.

The maximum FOV of the ASNOM system presented in Section 3 is 60μm x 60μm, thus in order to try and correlate far-field data to near-field data higher magnification was needed for CLSM imaging. In Fig. 2.c) and Fig. 2.d) we present 250μm x 250μm CLSM images collected using a 40X objective on the HE stained sample, and on its unstained counterpart, respectively. Manual registration of the two imaged regions was performed by selecting a reference feature on the micrographs collected at higher FOV, and setting the bottom-left corner of the 40X objective FOV at a specific fixed distance of this feature (~357 μm); the same registration procedure was applied for both stained and unstained samples. The FOV contained in the Fig. 2.c) and Fig. 2.d) micrographs corresponds to the larger yellow square areas depicted in Fig. 2.a) and Fig. 2.b), respectively. The inset in the top-right corner of Fig. 2.d) represents a TPEF image collected on the unstained instance on the same FOV as with CLSM. The tissue chromophores whose fluorescent emission contributed to the TPEF images that we collected under excitation with a 796 nm Ti:Sapphire laser beam are elastin, flavins, porphyrins, bilirubin and carotenoids. The reason for using both CLSM and TPEF on the unstained slide consisted in imaging signals from different endogenous chromophores in order to facilitate interpretation of collected s-SNOM & SHG-SNOM data.

After both stained and unstained slides were imaged by LSM, a CCD camera was used for cantilever positioning so as to enable ASNOM imaging on the unstained slide on regions that overlap with the FOVs imaged by LSM. A manual registration procedure similar to the one detailed in the previous paragraph was used in this purpose. Further on, AFM (Fig. 2.e), s-SNOM (Fig. 2.f) and SHG-SNOM (Fig. 2.g) images were collected on the unstained sample on a 60μm x 60μm region, corresponding to the position of the yellow rectangle of lower dimension depicted in Fig. 2.b). Thus, these regions imaged with ASNOM correspond to the bottom left corner of the CLSM & TPEF micrographs presented in Fig. 2.d).

In the CLSM micrograph collected on the HE stained sample under 40X magnification (Fig. 2.c) polygonal tumor cells with irregularly shaped nuclei, or without nuclei, can be observed. The plasma membrane, same as the cell nuclei, exhibits low (or no) fluorescent signals, thus the cells can be observed as being delimited by darker borders that entrap the abundant cytoplasm which yields high fluorescence emission under the 488nm illumination that we have used.

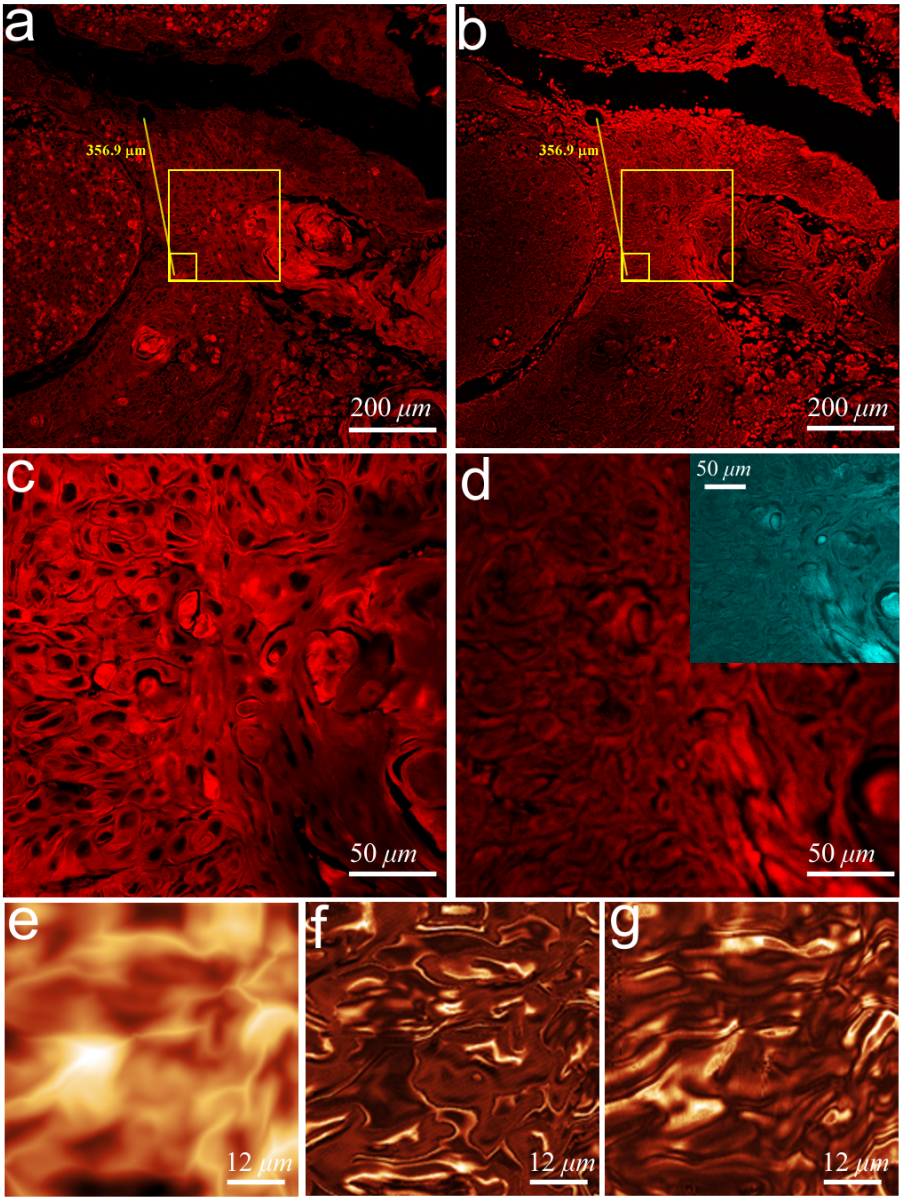

Fig. 2. Images collected on tissue fragments affected by SCC. Fluorescence CLSM images collected using a 10X objective on (a) HE stained and (b) unstained skin tissue fragments. The yellow square of higher dimension in (a) and (b) indicates the region where CLSM images were collected using a 40X objective on the (c) HE stained and (d) unstained samples. The inset in (d) represents a TPEF micrograph collected on the same FOV. The yellow square of lower dimension in (b) indicates the region of the unstained sample where images were collected by (e) AFM, (f) s-SNOM and (g) SHG-SNOM.

The shape of cells can be observed also in the case of the CLSM and TPEF images collected on the corresponding FOV on the unstained pair, but other histopathological cues, such as the shape of nuclei, or other aneuploidy related features are difficult to be observed. Although ASNOM images exhibit a good signal-to-noise ratio and polygonal shaped regions that might represent cells can be observed in the s-SNOM image (Fig. 2.f), and with reduced level of detail in the SHG-SNOM image (Fig. 2.g), in general, the content of ASNOM images is difficult to be placed into an obvious correspondence to the tissular elements imaged by CLSM and TPEF. One reason for this could consist in the influence of formaldehyde-fixation and paraffin-embedding. Processing the tissue sample by these methods that are routinely used for histopathology assays could be responsible for altering potential ASNOM signals of endogenous components or for introducing image elements linked to formaldehyde or paraffin related optical signals. In order to elucidate this aspect we have recently kicked-off a series of ASNOM imaging assays based on freshly excised, unprocessed, tissue fragments. Corroborating nanoscale information collected on skin tissue using complementary ASNOM techniques, such as s-SNOM, SHG-SNOM and FASNOM represents as well one of our future priorities in regard to imaging skin cancer via ASNOM.

Another aspect which is important to notice consists in the fact that the topography information recorded by AFM, Fig. 2.e), does not visually correlate to the information contained in the s-SNOM and SHG-SNOM images. This indicates clearly that the content recorded in the frame of our experiment by s-SNOM and SHG-SNOM is not affected by topographic artifacts, which many times affect ASNOM investigations. A challenging task for s-SNOM imaging was identifying sample regions with adequate roughness. High roughness yields difficulties in respect to maintaining the feedback of the piezoceramic element that controls sample (or probe) scanning; in the case of our imaging system height differences of over 5μm posing problems in this regard. Roughness related aspects prevented thus performing ASNOM imaging on some of the sample areas where it was attempted. This stands as the main reason for being unable to assemble a mosaic of ASNOM images to cover the whole area imaged by TPEF and CLSM. Although interpretation of the optical information that we have collected at nanoscale using s-SNOM and SHG-SNOM is yet to be resolved, the results of this reported experiment make us confident to believe that not long from now ASNOM techniques will begin to play an important role in tissue imaging. Whether best strategies in this regard will be based on exploiting optical signals generated by endogenous sources, or will require the coupling of exogenous agents, remains at this time an open question, one that we will endeavor to answer in future experiments.

5. Conclusions

The presented study introduces the concept of imaging skin tissue using ASNOM, and an imaging framework that could facilitate the correlation of ASNOM data with optical data collected using mature techniques (CLSM, TPEF), which are more accessible to pathologists in terms of interpretation. From a formaldehyde-fixed and paraffin-embedded skin tissue block affected by SCC pairs of consecutive tissue fragments were extracted. One of the sections in the pair was stained with HE and investigated using CLSM, while the second section in the pair was left unstained and imaged with CLSM, TPEF, s-SNOM and SHG-SNOM. While cues that allow tissues characterization with typical histopathology approaches are present in the CLSM & TPEF images, s-SNOM and SHG-SNOM data sets are more difficult to be interpreted based on traditional histopathology protocols. Interpretation of s-SNOM and SHG-SNOM data proved to be difficult, but we are confident that further cross-correlative studies similar to the presented experiment have the potential to advance the interpretation and understanding of ASNOM data collected on tissue samples, which once understood, could provide novel perspectives for cancer research.

Acknowledgments

The work of S.G. Stanciu and R. Hristu was supported by the Sectoral Operational Programme Human Resources Development (SOP-HRD), financed from the European Social Fund and the Romanian Government under the contract numbers POSDRU/159/1.5/S/137390 (S.G. Stanciu) and POSDRU/159/1.5/S/132397 (R. Hristu). The work of D.E. Tranca, M. Popescu, V. Enache and G.A. Stanciu was supported by the by the PN-II-PT-PCCA-2011-3.2-1162 Research Grant funded by UEFISCDI.

R E F E R E N C E S

[1] *P. Calzavara-Pinton, C. Longo, M. Venturini, R. Sala, and G. Pellacani*, "Reflectance Confocal Microscopy for In Vivo Skin Imaging", Photochemistry and photobiology 84, (2008), pp. 1421-1430.

[2] *J. Paoli, M. Smedh, A.M. Wennberg, and M.B. Ericson,* "Multiphoton laser scanning microscopy on non-melanoma skin cancer: Morphologic features for future non-invasive diagnostics", Journal of Investigative Dermatology 128, (2008), pp. 1248-1255.

[3] *S.K. Teh, W. Zheng, S.X. Li, D. Li, Y. Zeng, Y.Q. Yang, and J.A.Y. Qu*, "Multimodal nonlinear optical microscopy improves the accuracy of early diagnosis of squamous intraepithelial neoplasia", Journal of Biomedical Optics 18, (2013).

[4] *S. Seidenari, F. Arginelli, C. Dunsby, P. French, K. König, C. Magnoni, M. Manfredini, C. Talbot, and G. Ponti,* "Multiphoton laser tomography and fluorescence lifetime imaging of basal cell carcinoma: morphologic features for non-invasive diagnostics", Experimental dermatology 21 (2012), pp. 831-836.

[5] *R. Hillenbrand, B. Knoll, and F. Keilmann,* "Pure optical contrast in scattering-type scanning near-field microscopy", Journal of Microscopy-Oxford 202, (2001), pp. 77-83.

[6] *T.J. Yang, G.A. Lessard, and S.R. Quake,* "An apertureless near-field microscope for fluorescence imaging", Applied Physics Letters 76, (2000), pp. 378-380.
[7] *A.V. Zayats, and V. Sandoghdar,* "Apertureless near-field optical microscopy via local second-harmonic generation", Journal of Microscopy-Oxford 202, (2001), pp. 94-99.
[8] *N. Ocelic, A. Huber, and R. Hillenbrand,* "Pseudoheterodyne detection for background-free near-field spectroscopy", Applied Physics Letters 89, (2006), 101124.
[9] *S.G. Stanciu, D.E. Tranca, L. Tarpani, G.A. Stanciu, R. Hristu, and L. Latterini,* "Investigations on organic fluorophore doped silica nanoparticles by apertureless scanning near-field optical microscopy", Transparent Optical Networks (ICTON), 2014 16th International Conference on, (2014), pp. 1-4.
[10] *D. E. Tranca, S. G. Stanciu, R. Hristu, C. Stoichita, S.A.M. Tofail, and G.A. Stanciu,* "High-resolution quantitative determination of dielectric function by using scattering scanning near-field optical microscopy", Scientific Reports 5, (2015), 11876.
[11] *M.R. Castellanos, A. Szerszen, S. Gundry, E.C. Pirog, M. Maiman, S. Rajupet, J.P. Gomez, A. Davidov, P.R. Debata, and P. Banerjee,* "Diagnostic imaging of cervical intraepithelial neoplasia based on hematoxylin and eosin fluorescence", Diagnostic pathology 10, (2015), 119.